Analytical Modeling of Switching Energy of Silicon Carbide Schottky Diodes as Functions of dI_{DS}/dt and Temperature

Saeed Jahdi, *Student Member, IEEE*, Olayiwola Alatise, *Member, IEEE*, Li Ran, *Senior Member, IEEE*,
and Philip Mawby, *Senior Member, IEEE*

***Abstract*—SiC Schottky Barrier diodes (SiC SBD) are known to oscillate/ring in the output terminal when used as free-wheeling diodes in voltage-source converters. This ringing is due to RLC resonance among the diode capacitance, parasitic resistance, and circuit stray inductance. In this paper, a model has been developed for calculating the switching energy of SiC diodes as a function of the switching rate (dI_{DS}/dt of the commutating SiC MOSFET) and temperature. It is shown that the damping of the oscillations increases with decreasing temperature and decreasing dI_{DS}/dt. This in turn determines the switching energy of the diode, which initially decreases with decreasing dI_{DS}/dt and subsequently increases with decreasing dI_{DS}/dt thereby indicating an optimal dI_{DS}/dt for minimum switching energy. The total switching energy of the diode can be subdivided into three phases namely the current switching phase, the voltage switching phase, and the ringing phase. Although the switching energy in the current switching phase decreases with increasing switching rate, the switching energy of the voltage and ringing phase increases with the switching rate. The model developed characterizes the dependence of diode's switching energy on temperature and dI_{DS}/dt, hence, can be used to predict the behavior of the SiC SBD.**

***Index Terms*—Analytical modeling, device characterization, Schottky barrier diode (SBD), silicon carbide, switching energy.**

NOMENCLATURE

V_{AK}	Diode voltage (V).
V_{AKpk}	Peak diode voltage overshoot (V).
V_{DD}	Supply (input) voltage (V).
V_{d}	Diode on-state voltage drop (V).
V_{TH}	Diode threshold voltage (V).
V_{GG}	MOSFET gate voltage (V).
V_{GS}	MOSFET gate source voltage (V).
dV_{AK}/dt	*dV/dt* of turn-OFF voltage of diode (V/s).
I_{AK}	Diode current (A).
I_{F}	Diode forward current (A).
I_{PR}	Diode peak reverse current (A).
I_{DS}	MOSFET current (A).
dI_{DS}/dt	*dI/dt* of turn-ON current of mosfet (turn-OFF of diode) (A/s).
L_{STRAY}	Stray parasitic inductance (H).
L_{E}	Circuit energizing inductor (H).
C_{iss}	MOSFET input capacitance (F).
C_{GD}	MOSFET Miller capacitance (F).
C_{AK}	Diode depletion capacitance (F).
R_{AK}	Diode depletion resistance (Ω).
R_{S}	Parasitic series resistance (Ω).
R_{G}	MOSFET gate resistance (Ω).
α	Neper frequency (attenuation factor) of diode response (s^{-1}).
ω	Oscillations (swing) frequency (rad/s).
ζ	Damping factor of diode responde (–).
L	Channel length in device (μm).
W	Channel width in device (μm).
μ	Effective mobility of carriers (cm^2/Vs).
C_{OX}	Effective capacitance density (fF/$\mu\mathrm{m}^2$).
E_{SW}	Switching energy (J).
T	Temperature (°C).
t	Time (s).

I. INTRODUCTION

SILICON Carbide Schottky barrier diodes (SiC SBD) have shown significant improvements in the performance of rectifiers compared with traditional silicon PiN diodes. The physics and structure of the SiC SBD is presented in [1]–[3], where considerable advantages in terms of higher switching speed, significant reduction in reverse recovery, and better electrothermal performance in harsh environments have been presented [4]. It has previously been shown that the application of SiC SBDs as rectifiers rather than conventional silicon PiN diodes can significantly reduce thermal stress, lower power losses, [5] and enhance the conversion efficiency by removing the reverse recovery of the PiN in the switching transients [6]. As a result, their application as rectifiers in power converters is getting more popular [7]. These include power converters for a range of applications [8] such as power factor correction circuits [9], high power converters [10], [11], and also in harsh environments such as in space applications [12]. Schottky diodes are also used to block the unwanted conduction of the MOSFET body diodes during dead times in power converters [13]. In addition, switching combinations of SiC Schottky diodes with various transistors including silicon power MOSFETs [14], CoolMOS [15], SiC MOSFETs [16], [17], and JFETs [18] have shown significant advantages compared to that of combinations with silicon PiN diodes [19].

Manuscript received March 6, 2014; revised May 8, 2014; accepted June 11, 2014. Date of publication June 26, 2014; date of current version January 16, 2015. Recommended for publication by Associate Editor A. Lindemann.

The authors are with the Department of Electrical and Electronics Engineering, School of Engineering, University of Warwick, Coventry CV4 7AL, U.K. (e-mail: s.jahdi@warwick.ac.uk; o.alatise@warwick.ac.uk; l.ran@warwick.ac.uk; p.a.mawby@warwick.ac.uk).

Color versions of one or more of the figures in this paper are available online at http://ieeexplore.ieee.org.

Digital Object Identifier 10.1109/TPEL.2014.2333474

TABLE I
PARAMETERS AND VALUES

V_{TH}	4 V
V_{GS}	18 V
V_{DD}	100 V
C_{GD}	152 pF
C_{AK}	250 pF
C_{iss}	3690 pF
L_{STRAY}	1500 nH
L_{E}	7.4 mH
R_{S}	2.5 Ω
R_{AK}	10 kΩ
R_{G}	10 Ω–1000 Ω
T	–75 °C –175 °C

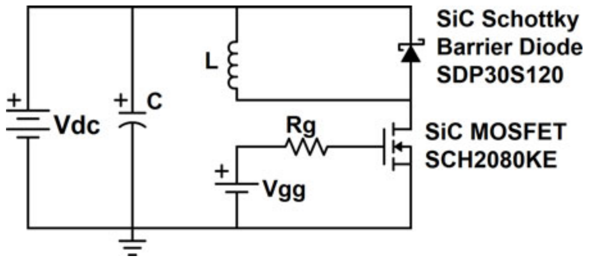

Fig. 1. Schematic of the clamped inductive switching test rig.

Although SiC diodes do not exhibit reverse recovery like PiN diodes, they are, however, prone to electromagnetic oscillations or ringing in the output voltage. This ringing is due to the interaction between the diode depletion capacitance and the stray inductance of the circuit and packaging. These oscillations will impact electromagnetic interference, reliability, and protection circuitry of the devices when used in applications like power converters. The ringing characteristics are sensitive to temperature variations and the switching rate of the commutating transistor. Previously reported research on the switching characteristics of SiC SBDs has focused on temperature invariance at high switching rates [20], whereas at lower switching rates, the switching characteristics of the SiC SBD become more temperature sensitive. The damping of the oscillations is strongly temperature dependent in SiC Schottky diodes, whereas the oscillation frequency is dependent on the parasitic inductance and depletion capacitance of the diode. Hence, there is a need for accurate switching energy modeling techniques that can account for ringing in SiC Schottky diodes.

The models that have previously been developed to understand the transient behavior of silicon PiN diodes during reverse recovery, including physics-based models [21], [22], analytical models [23]–[25], Saber Models [26], and PSPICE Models [27] are not extendable to SiC Schottky diodes since the latter is unipolar [28]. Models for parameter extraction in SiC Schottky diodes [29] provide valuable information about understanding the static behavior of the diodes, however, they lack the capability of modeling dynamic characteristics and switching energy. As unipolar devices do not rely on conductivity modulation from minority carrier injection within the device, modeling them seems to be less complex; however, there are modeling challenges arising from the dependence of diode ringing on the parasitic elements, temperature, and the commutation rate of the transistor.

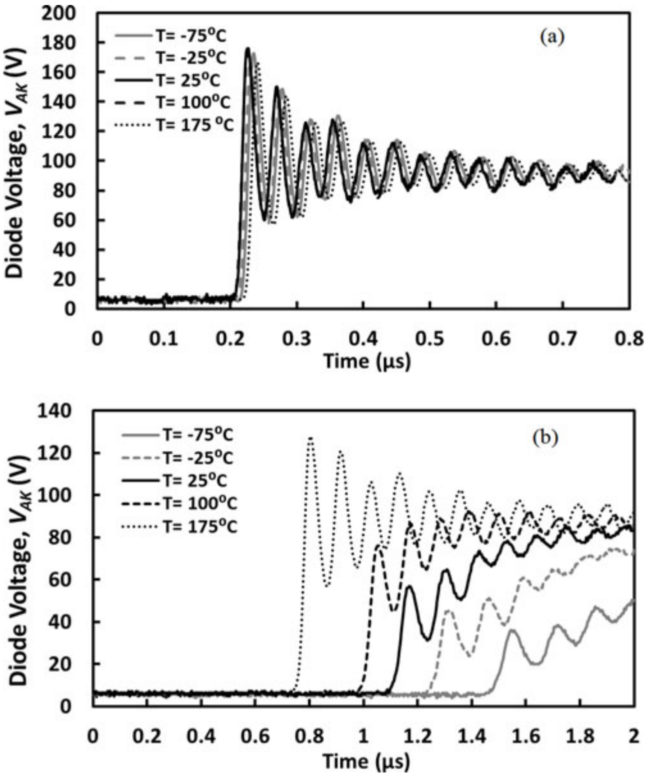

Fig. 2. Measured turn-OFF Voltage of SiC schottky diode, dI_{DS}/dt is modulated by (a) $R_{\mathrm{G}} = 15\ \Omega$ and (b) 150 Ω.

There have been previous reports on the impact of stray parameters on the static and dynamic performance of the Schottky diode [30]. In this paper, an analytical model for turn-OFF switching transients of SiC SBD is presented, evaluated, and validated through experimental measurements. The models are proven to be able to accurately predict the switching energy of the SiC Schottky diodes through a wide range of temperatures and switching rates modulated by the silicon carbide MOSFET acting as the low-side transistor. Section II shows the experimental measurements setup and results; Section II shows the details of the development of the model; Section I shows the validation of the model, while Section V concludes the paper.

II. EXPERIMENTAL MEASUREMENTS

The experimental measurements are performed in the classic quasi switching manner using a double-pulsed clamped inductive switching test rig with the schematic shown in Fig. 1. The actual test rig is shown in [31]. The measurements are performed on a 1.2-kV/30-A SiC Schottky barrier diode with datasheet reference SDP30S120. The low-side transistor is a SiC MOSFET with datasheet reference SCH2080KE. The switching rates are modulated by a range of gate resistances and the temperature has been varied within a range of –75 °C to 175 °C.

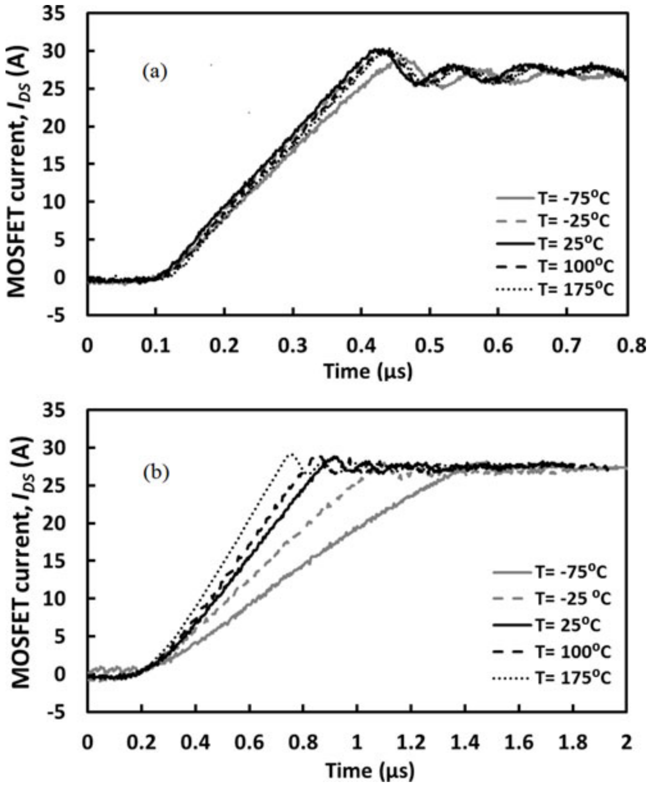

Fig. 3. Measured turn-OFF current of SiC MOSFET, where the dI_{DS}/dt is modulated by (a) $R_G = 15\ \Omega$ and (b) 150 Ω on the low-side MOSFET. Measurements show that dI_{DS}/dt increases with temperature and higher variations with temperature are for higher R_G.

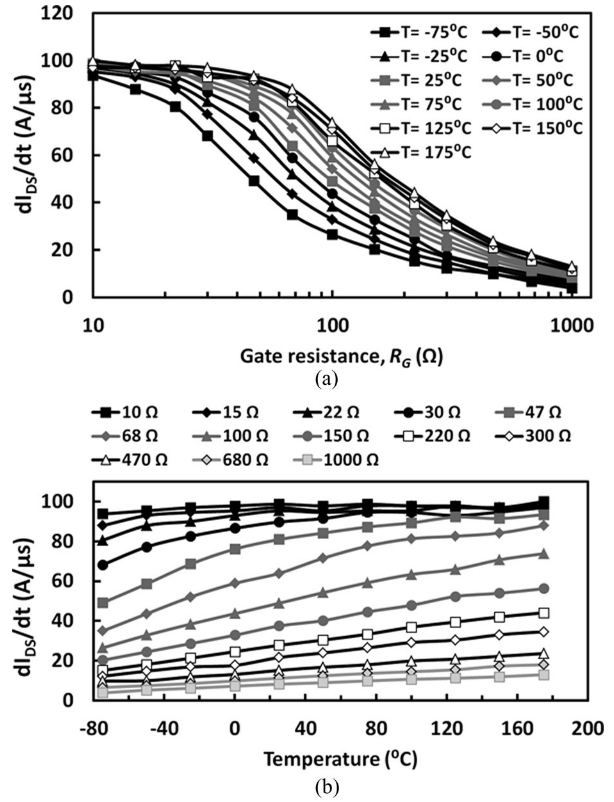

Fig. 4. Measured dI_{DS}/dt as a functions of (a) gate resistance and (b) temperature showing that dI_{DS}/dt increases with temperature.

Fig. 2(a) shows the diode turn-OFF voltage characteristics for different temperatures when the low-side SiC MOSFET is switched with a 15-Ω gate resistance. Fig. 2(b) shows the diode voltage characteristics switched with 150-Ω gate resistance. Fig. 3(a) and (b) shows the MOSFET drain current transient during turn-ON of the MOSFET (turn-OFF of the diode) for $R_{\mathrm{G}} = 15\ \Omega$ and $R_{\mathrm{G}} = 150\ \Omega$, respectively, at different temperatures. It can be seen that the temperature dependence of the diode voltage characteristics is higher with the higher gate resistance, i.e., $d^2 I_{\mathrm{DS}}/dtdT$ increases as $\mathrm{R_G}$ is increased from 15 to 150 Ω. It can also be seen from Fig. 2(a) and (b) that the damping of the diode ringing increases as the temperature decreases. This is due to the fact the dI_{DS}/dt increases with increasing temperature and diode ringing oscillations become less damped as dI_{DS}/dt increases. It can be seen that dI_{DS}/dt increases with increasing temperature. Fig. 4(a) and (b) shows the measured dI_{DS}/dt as a function of R_{G} for different temperatures and dI_{DS}/dt as a function of temperature, respectively.

III. MODEL DEVELOPMENT

A. Characterization of Diode Ringing

The context of modeling the switching transient of the SiC Schottky diodes is the clamped inductive switching circuit. Fig. 5 shows the circuit with the diode acting as a high-side free-wheeling diode with a low-side transistor, which in this paper is a 1.2-kV SiC MOSFET. The diode, during the switching transient, is modeled as a depletion capacitance (C_{AK}), a depletion resistance (R_{AK}), a series parasitic resistance (R_{S}), and a stray inductance (L_{stray}). The depletion capacitance is due to the voltage dependent depletion width (between the Schottky metal and the voltage blocking semiconductor), which increases as the voltage across the diode increases. Since this capacitance varies with the voltage across the diode through the depletion width, the value of C_{AK} used is calculated from the average capacitance measured over the voltage range. The corresponding depletion resistance is due to the finite resistance of the depletion width, i.e., the depletion capacitance is modeled as a lossy capacitor. The finite resistance of the depletion width (R_{AK}) is due to the fact that there is a nonzero conductance as was determined by capacitance–voltage measurements. This can be due to prebreakdown avalanche multiplication caused by free carriers under the influence of the increasing electric field. The current through the depletion width can also be caused by thermionic emission across the Schottky interface. The highest depletion capacitance across the diode is formed when the voltage across it is at a minimum, i.e., at the instant that reverse voltage starts increasing. As the reverse bias across the diode increases due to the switching transient, the depletion capacitance will reduce as the depletion width increases; hence, the depletion capacitance used in the model was an average depletion capacitance which can be measured by the capacitance-voltage (CV) curves performed at lower voltages. These are shown in

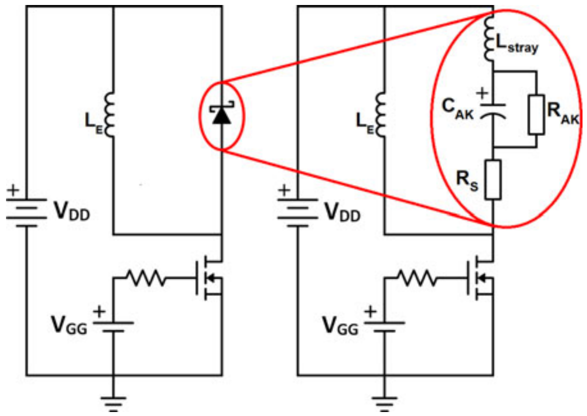

Fig. 5. SBD model in the test rig.

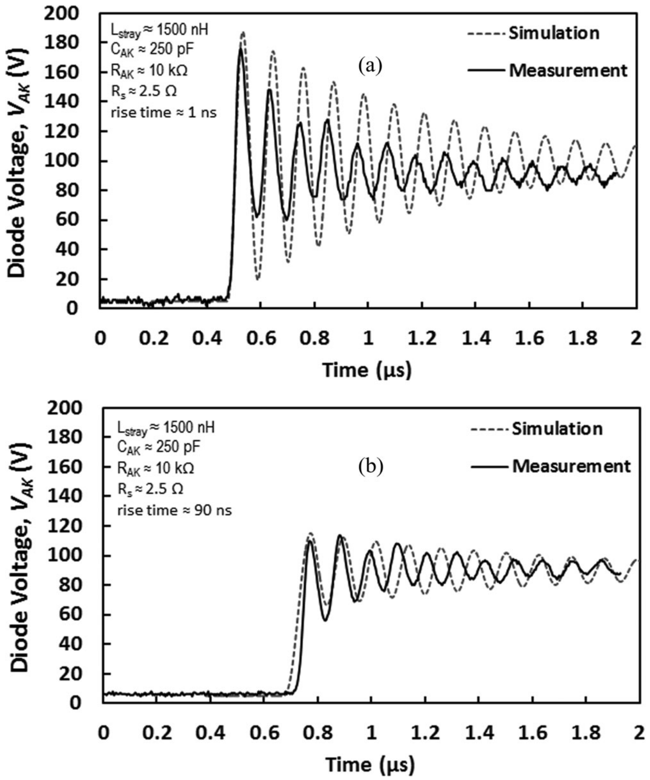

Fig. 6. Measured and modeled voltage at turn-OFF of SiC Schottky diode where switching speeds are modulated by (a) $R_G = 15\ \Omega$ and (b) $R_G = 150\ \Omega$.

Table 1. This average junction capacitance is used to determines the behavior of the devices [10], [11]. The parameters of this circuit have been varied within reasonable margins to obtain matching. The values for the depletion capacitance and resistances are obtainable as average values as discussed. The stray inductance and the series resistance are also due to the packaging and circuit wiring which here are significantly high due to the wirings to the thermal chamber. The equivalent circuit of the diode has been modeled in a circuit simulator (Multisim 12.0) using these parameters to provide a matching for the experiments. Fig. 6(a) and (b) shows the ringing characteristics of the diode output voltage switched at two different rates. In Fig. 6(a), the low-side SiC MOSFET is switched with a 15-Ω gate resistor, whereas in Fig. 6(b), the low-side MOSFET is switched with a gate resistance of 150 Ω. It can be seen from Fig. 6 that there is reasonably good matching between the measured and modeled characteristics. Fig. 6 shows, as expected, that the peak voltage overshoot during turn-OFF increases with the switching rate (due to a higher $L.dI_{\mathrm{DS}}/dt$) and the damping is less when the switching rate is higher.

As the low-side MOSFET is switched ON and the high-side diode is switched OFF, the power supply voltage is to be applied across the diode as it begins to block. The switching of this voltage across the diode can be modeled as an input into the transfer function of the diode. The diode output voltage can then be modeled as the product of the diodes transfer function and the input voltage. In this regard, the equivalent circuit of the diode can be represented as a second-order RLC circuit with a transfer function H(s) that can easily be derived by taking the ratio of the voltage across the diode to the input voltage. The diode output voltage is the product of the input voltage and the transfer function. Therefore, by driving the diode output voltage, the results will be as shown in (1), where

$$\begin{aligned} V_{\mathrm{AK}} &= \frac{V_{\mathrm{DD}}}{1+sR_G C_{\mathrm{GD}}} H(s) \\ &= \frac{V_{\mathrm{DD}}}{1+sR_G C_{\mathrm{GD}}} \\ &\quad \times \frac{s\left(\frac{R_S}{L_{\mathrm{Stray}}}\right) + \frac{R_{\mathrm{AK}}+R_S}{L_{\mathrm{stray}} R_{\mathrm{AK}} C_{\mathrm{AK}}}}{s^2 + s\left(\frac{R_{\mathrm{AK}} R_S C_{\mathrm{AK}} + L_{\mathrm{stray}}}{L_{\mathrm{stray}} R_{\mathrm{AK}} C_{\mathrm{AK}}}\right) + \frac{R_{\mathrm{AK}}+R_S}{L_{\mathrm{stray}} R_{\mathrm{AK}} C_{\mathrm{AK}}}}. \end{aligned} \tag{1}$$

In (1), the input voltage does not appear across the diode as a step function (instantaneously) but rather as an exponential with a time constant equal to the electrical time constant ($R_{\mathrm{G}} C_{\mathrm{GD}}$) of the bottom-side switching MOSFET. The product $R_{\mathrm{G}} C_{\mathrm{GD}}$ is approximately the time required for the Miller capacitance of the MOSFET is charge during the plateau stage of the gate voltage transient at turn-on. As the Miller capacitance changes with the voltage during the diode turn-OFF transient, thereby C_{GD} here represents an average value of the overall capacitance [10]. The Miller capacitance is charged when the drain voltage (V_{DD}) across the bottom side MOSFET falls from the supply voltage to the on-state voltage and the voltage across the diode rises from the on-state voltage drop to the input voltage. The switching rate of the bottom-side MOSFET (dI_{DS}/dt) is also the rate at which current is commutated away from the high-side diode, hence, the rate at which the SBD diode is turned OFF. The on-state current of the low-side MOSFET can be expressed by (2) below

$$I_{\mathrm{DS}} = \frac{B}{2}\left(V_{\mathrm{GS}} - V_{\mathrm{TH}}\right)^2 \tag{2}$$

where

$$B = \frac{W\mu C_{\mathrm{OX}}}{L}$$

and

$$V_{\mathrm{GS}} = V_{\mathrm{GG}}\left(1 - \exp\left(-\frac{t}{R_G C_{\mathrm{iss}}}\right)\right). \tag{3}$$

By taking the derivative of (2) against time, the turn-ON switching rate of the low-side MOSFET can be expressed as

$$\frac{dI_{\mathrm{DS}}}{dt} = B\left(V_{\mathrm{GS}} - V_{\mathrm{TH}}\right)\frac{V_{\mathrm{GG}}}{R_G C_{\mathrm{iss}}}\exp\left(-\frac{t}{R_G C_{\mathrm{iss}}}\right). \tag{4}$$

The parameters used in the calculation of (4) are taken from the MOSFET datasheet. As can be seen from (4), the switching rate is time dependent and decreases as the switching time increases. At the point of maximum dI_{DS}/dt, (4) can be rewritten (assuming that t is small enough with respect to $R_{\mathrm{G}}C_{\mathrm{iss}}$ for the exponential to be unity) in terms of R_{G} as

$$R_G = \frac{B(V_{\mathrm{GS}} - V_{\mathrm{TH}})V_{\mathrm{GG}}}{C_{\mathrm{iss}}\left(\frac{dI_{\mathrm{DS}}}{dt}\right)}. \tag{5}$$

Substituting (5) into (1) yields an expression for the diode voltage in terms of the switching rate

$$V_{AK} = A \times \frac{s\left(\frac{R_S}{L_{\mathrm{Stray}}}\right) + \frac{R_{\mathrm{AK}} + R_S}{L_{\mathrm{stray}} R_{\mathrm{AK}} C_{\mathrm{AK}}}}{s^2 + s\left(\frac{R_{\mathrm{AK}} R_S C_{\mathrm{AK}} + L_{\mathrm{stray}}}{L_{\mathrm{stray}} R_{\mathrm{AK}} C_{\mathrm{AK}}}\right) + \frac{R_{\mathrm{AK}} + R_S}{L_{\mathrm{stray}} R_{\mathrm{AK}} C_{\mathrm{AK}}}} \tag{6}$$

where A can be defined as

$$A = \frac{\frac{dI_{\mathrm{DS}}}{dt} V_{\mathrm{DD}}}{\frac{dI_{\mathrm{DS}}}{dt} + s\left(\frac{BV_{\mathrm{GG}}(V_{\mathrm{GS}} - V_{\mathrm{TH}})}{C_{\mathrm{iss}}} C_{\mathrm{GD}}\right)}.$$

Equation (6) will be instrumental in the development of the switching energy model for the SiC Schottky diode since it will be needed to determine the oscillations behavior. From the coefficients of denominator in (6), the attenuation or Neper frequency α_{V}, the frequency of the oscillations ω and the damping factor ζ of SiC schottky diode voltage can be derived as

$$\alpha_V = \frac{R_{\mathrm{AK}} R_S C_{\mathrm{AK}} + L_{\mathrm{stray}}}{2L_{\mathrm{stray}} R_{\mathrm{AK}} C_{\mathrm{AK}}} \tag{7a}$$

$$\omega = \sqrt{\frac{R_{\mathrm{AK}} + R_S}{L_{\mathrm{stray}} R_{\mathrm{AK}} C_{\mathrm{AK}}}} \tag{7b}$$

$$\zeta = \frac{\alpha_V}{\omega} = \frac{R_S R_{\mathrm{AK}} C_{\mathrm{AK}} + L_{\mathrm{Stray}}}{2\sqrt{R_{\mathrm{AK}} L_{\mathrm{Stray}} C_{\mathrm{AK}}(R_S + R_{\mathrm{AK}})}}. \tag{7c}$$

Experimentally, it is seen in Fig. 7 that the oscillations frequency of the diode current have approximately the same frequency as its voltage; however, its decay attenuation is higher (here, for approximately two times). Therefore, in Fig. 10, the current is also shown to damp faster.

B. Switching Energy Model

The expressions for the oscillation frequency ω and attenuation α will be used in the development of the diode switching energy model. Fig. 7(a) shows the experimental measurements of the diode current and voltage during turn-OFF with the low-side SiC MOSFET switched with a gate resistance of 15 Ω. Fig. 7(b) shows experimental measurements of the diode current and voltage when the low-side SiC MOSFET is switched more slowly with a gate resistance of 150 Ω. When comparing Fig. 7(a) and (b), it can be seen that the ringing is dramatically reduced as the switching rate (dI_{DS}/dt) is reduced; however, the switching duration of the current increased. Fig. 8(a) shows the switching power transient as a function of time for $R_{\mathrm{G}} = 15$ Ω, whereas Fig. 8(b) shows the same plot for $R_{\mathrm{G}} = 150$ Ω. It can be seen from Fig. 8(a) that when the diode is switched with a higher MOSFET dI_{DS}/dt, the oscillations in the diode voltage cause additional power peaks beyond the main peak. These additional power peaks will add to the switching energy of the diode. In Fig. 8(b), the switching power transient does not contain such additional power peaks due to ringing, although the dissipated power associated with the switching current is larger. In order to correctly modeling the switching energy of the diode, it will be important to capture these peaks in the modeling and account for how the peaks change with the switching rate and temperature. The integration of these power peaks over time will yield the total switching energy. Fig. 9(a) shows measurements of the 15-Ω switching power transients at different temperatures showing that the switching energy is largely temperature invariant in Schottky diodes. Fig. 9(b) also shows a similar plot for the R_{G} = 150 Ω.

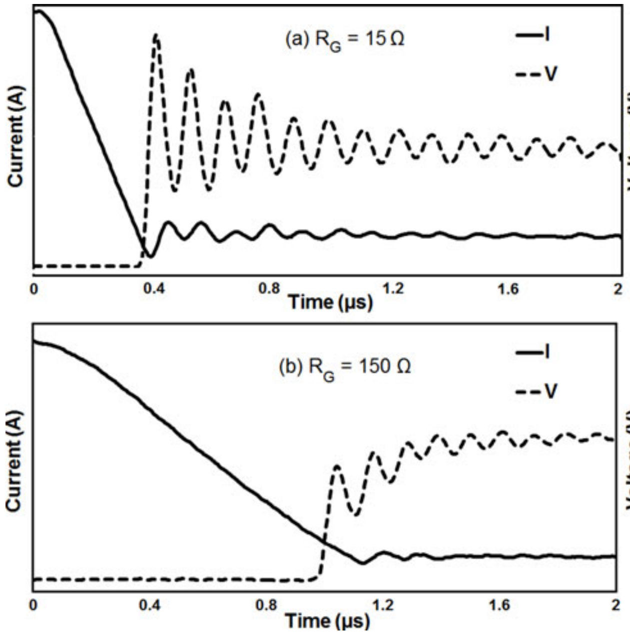

Fig. 7. Current and voltage waveforms of SiC SBD at turn-OFF at 25 °C with (a) $R_{\mathrm{G}} = 15$ Ω and (b) $R_{\mathrm{G}} = 150$ Ω.

The analytical model for the switching energy is based on approximating the waveforms by mathematical functions and integrating them over the transient duration. Fig. 10 shows these approximations for the current and voltage waveforms of the SiC diode. The switching energy is divided into three sections namely the current switching phase, the voltage switching phase, and the ringing phase. In Section I (the current switching

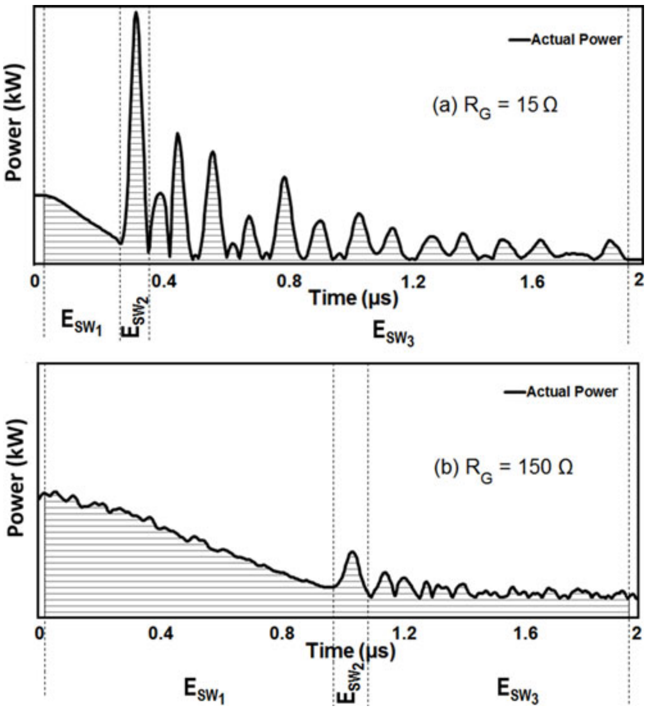

Fig. 8. Comparison of waveforms of the transient power of SiC SBD with (a) $R_{\mathrm{G}} = 15\ \Omega$ and (b) $R_{\mathrm{G}} = 150\ \Omega$.

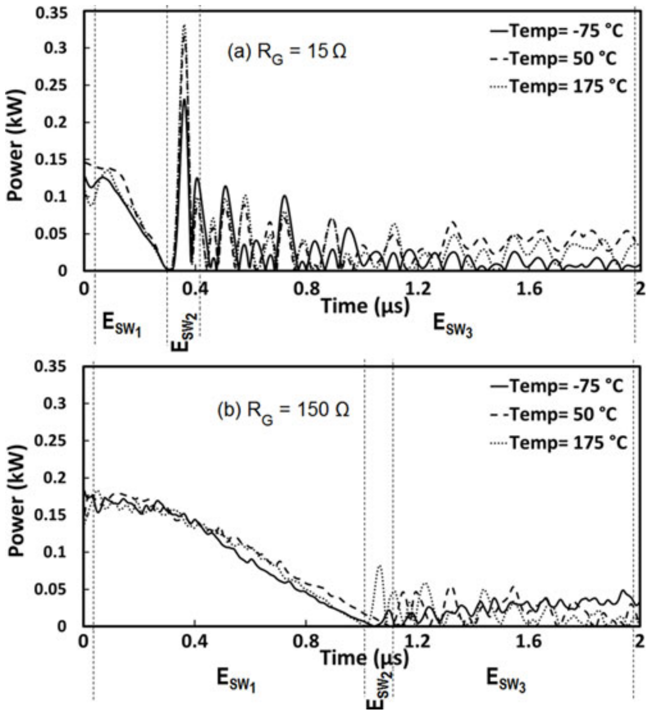

Fig. 9. Measured transient power at different temperatures of SiC SBD with (a) $R_{\mathrm{G}} = 15\ \Omega$ and (b) $R_{\mathrm{G}} = 150\ \Omega$.

phase), between t_1 and t_2, the current is approximated as a linear function with a negative derivative, while the diode voltage is constant at the on-state voltage drop (V_{d}). It is assumed that the current overshoots with the same rate and goes negative at the same instant then the diode voltage starts to rise. This is based on thae fact that the bottom-side MOSFET attains the load current at the instant that the Miller capacitance has finished charging, and the drain-source voltage across the MOSFET falls from the input voltage to the on-state voltage. The measured waveforms in Fig. 7 show that this is indeed the case. The switching energy calculated for Section I. which is E_{SW1} (the current switching phase) is simply the integration of the switching power from t_1 (the initial point) to t_2

$$E_{\mathrm{SW1}} = \int_{t_1}^{t_2} \left(I_F - \frac{dI_{\mathrm{DS}}}{dt} t\right) V_d \, dt = \frac{V_d I_F^2}{2\frac{dI_{\mathrm{DS}}}{dt}} \tag{8}$$

where

$$t_1 = 0 \quad \text{and} \quad t_2 = \frac{I_F}{\frac{dI_{\mathrm{DS}}}{dt}}.$$

In Section II. (the voltage switching phase), which spans from t_2 to t_3, the diode voltage is approximated as a linear function with a positive derivative that rises from the on-state voltage of the diode to the peak voltage, which is the sum of the input voltage and the inductive overshoot. It is also assumed that the current through the diode reaches its peak negative value at the same instant having the same dI_{DS}/dt. Therefore current equations in E_{SW1} and E_{SW2} are the same while the voltage enters a new phase. Based on analyzing the experimental measurements, additional terms such as Peak reverse current I_{PR} and peak voltage overshoot V_{AKpk} are also introduced to assist in determining the switching energy. The equation for the switching energy in the voltage switching phase E_{SW2} is simply the integration of the switching power from t_2 to t_3 which is shown in (9) at the bottom of this page,where

$$t_3 = \frac{I_F}{\frac{\mathrm{d}I_{\mathrm{DS}}}{\mathrm{d}t}} + \frac{V_{\mathrm{AKpk}} - V_d}{\frac{\mathrm{d}V_{\mathrm{AK}}}{\mathrm{d}t}}.$$

$$\begin{aligned} E_{\mathrm{SW2}} &= \int_{t_2}^{t_3} \left(I_F - \frac{dI_{\mathrm{DS}}}{dt} t\right) \left(\frac{dV_{\mathrm{AK}}}{dt} t - \frac{I_F}{\frac{dI_{\mathrm{DS}}}{dt}} \frac{dV_{\mathrm{AK}}}{dt} + V_d\right) dt \\ &= \left. \frac{-dI_{\mathrm{DS}}}{dt} \frac{dV_{\mathrm{AK}}}{dt} \frac{t^3}{3} + \frac{t^2 \left(V_d \left(\frac{dI_{\mathrm{DS}}}{dt}\right)^2 - 2I_F \frac{dV_{\mathrm{AK}}}{dt} \frac{dI_{\mathrm{DS}}}{dt}\right)}{2\frac{dI_{\mathrm{DS}}}{dt}} - \frac{t\left(\frac{dV_{\mathrm{AK}}}{dt} I_F^2 - V_d \frac{dI_{\mathrm{DS}}}{dt} I_F\right)}{\frac{dI_{\mathrm{DS}}}{dt}} \right|_{t_2}^{t_3} \\ &= \frac{dI_{\mathrm{DS}}}{dt} \frac{(V_{\mathrm{AKpk}} - V_d)^2 (2V_{\mathrm{AKpk}} + V_d)}{6\left(\frac{dV_{\mathrm{AK}}}{dt}\right)^2} \end{aligned} \tag{9}$$

In Section III. (the ringing phase), which is from t_3 to t_4, both the diode current and voltage are modeled as damped sinusoids with a defined oscillation frequency and damping. The oscillation frequency and damping of the diode voltage has been determined previously.

The limits for the integration over Section II. is taken to be the five times the time constant of the oscillations decaying exponential, so

$$t_4 = \gamma + \frac{V_{\mathrm{AKpk}} - V_d}{\frac{dV_{\mathrm{AK}}}{dt}} + \frac{I_F}{\frac{dI_{\mathrm{DS}}}{dt}}$$

in which γ is

$$\gamma = \frac{5}{\alpha_V} = \frac{10 L_{\mathrm{stray}} R_{\mathrm{AK}} C_{\mathrm{AK}}}{R_{\mathrm{AK}} R_S C_{\mathrm{AK}} + L_{\mathrm{stray}}}.$$

The ringing in the circuit is determined by the parasitic inductance and capacitance associated with the Schottky diode and, hence, will depend on the parameters such as α and ω . The equation for the switching energy in Section III. after the insertion of the limits in (10) is shown at the bottom of the page in (11).

The total switching energy (E_{SWtotal}) in the diode will be the sum of the absolute values of E_{SW1}, $\mathrm{E}_{\mathrm{SW2}}$, and E_{SW3} as presented in Fig. 10. Given the diode current, voltage, dI_{DS}/dt, dV_{AK}/dt, and RLC values of the diode equivalent circuit, the switching energy can be calculated as a function of the switching rate

$$E_{\mathrm{SWtotal}} = E_{\mathrm{SW1}} + E_{\mathrm{SW2}} + E_{\mathrm{SW3}}.$$

Fig. 10 shows the modeled switching power transient, which is a good approximation of the measured switching power transient in Fig. 9.

C. Incorporating Temperature Dependency

To incorporate temperature dependency into the switching energy model, the temperature dependency of the switching rate will have to be determined first. The temperature dependency

---

$$\begin{aligned} E_{\mathrm{SW3}} &= \int_{t_3}^{t^4} I_{\mathrm{PR}} e^{-\alpha_I t} \sin(\omega t) \left(V_{\mathrm{DD}} + L \frac{dI_{\mathrm{DS}}}{dt} e^{-\alpha_V t} \sin(\omega t) \right) dt \\ &= -\Bigg(\frac{I_{\mathrm{PR}} V_{\mathrm{DD}} (\alpha_I \sin(\omega t) + \omega \cos(\omega t))}{e^{\alpha_I t} (\alpha_I^2 + \omega^2)} \\ &\quad - \frac{I_{\mathrm{PR}} L \frac{dI_{\mathrm{DS}}}{dt} ((\alpha_I + \alpha_V) \cos(2\omega t) - 2\omega \sin(2\omega t))}{2e^{(\alpha_I + \alpha_V)} ((\alpha_I + \alpha_V)^2 + 4\omega^2)} + \frac{I_{\mathrm{PR}} L \frac{dI_{\mathrm{DS}}}{dt}}{2e^{(\alpha_I + \alpha_V)t} (\alpha_I + \alpha_V)} \Bigg) \Bigg|_{t_3}^{t_4} \end{aligned} \tag{10}$$

$$\begin{aligned} E_{\mathrm{SW3}} = {} & \frac{L I_{\mathrm{PR}} \frac{\mathrm{d}I_{\mathrm{DS}}}{\mathrm{d}t} e^{(\alpha_I + \alpha_V)\left(\frac{V_d}{\frac{dV_{AK}}{dt}}\right)} (e^{(\alpha_l + \alpha_V)\gamma} - 1)}{2(\alpha_I + \alpha_V) e^{(\alpha_I + \alpha_V)\gamma + \frac{(\alpha_I + \alpha_V) I_F}{\frac{dI_{\mathrm{DS}}}{dt}} + \frac{(\alpha_I + \alpha_V)(V_{\mathrm{AKpk}})}{\frac{dV_{\mathrm{AK}}}{dt}}}} \\ & - I_{\mathrm{PR}} V_{\mathrm{DD}} \left(\left(\frac{\alpha_I \sin\left(\omega \left(\frac{I_F}{\frac{dI_{\mathrm{DS}}}{dt}} + \frac{V_{\mathrm{AKpk}} - V_d}{\frac{dV_{AK}}{dt}} + \gamma\right)\right) + \omega \cos\left(\omega \left(\frac{I_F}{\frac{dI_{DS}}{dt}} + \frac{V_{\mathrm{AKpk}} - V_d}{\frac{dV_{\mathrm{AK}}}{dt}} + \gamma\right)\right)}{(\alpha_I^2 + \omega^2)\, e^{\alpha_I \left(\frac{I_F}{\frac{dI_{\mathrm{DS}}}{dt}} + \frac{V_{\mathrm{AKpk}} - V_d}{\frac{dV_{\mathrm{AK}}}{dt}} + \gamma\right)}} \right) \right. \\ & \left. - \left(\frac{\alpha_I \sin\left(\omega \left(\frac{I_F}{\frac{dI_{\mathrm{DS}}}{dt}} + \frac{V_{\mathrm{AKpk}} - V_d}{\frac{dV_{\mathrm{AK}}}{dt}}\right)\right) + \omega \cos\left(\omega \left(\frac{I_F}{\frac{dI_{\mathrm{DS}}}{dt}} + \frac{V_{\mathrm{AKpk}} - V_d}{\frac{dV_{\mathrm{AK}}}{dt}}\right)\right)}{(\alpha_I^2 + \omega^2) e^{\alpha_I \left(\frac{I_F}{\frac{dI_{\mathrm{DS}}}{dt}} + \frac{V_{\mathrm{AKpk}} - V_d}{\frac{dV_{\mathrm{AK}}}{dt}}\right)}} \right) \right) \\ & + \left(\frac{L I_{\mathrm{PR}}}{2} \frac{dI_{\mathrm{DS}}}{dt} \left(\frac{(\alpha_I + \alpha_V) \cos\left(2\omega \left(\frac{I_F}{\frac{dI_{\mathrm{DS}}}{dt}} + \frac{V_{\mathrm{AKpk}} - V_d}{\frac{dV_{\mathrm{AK}}}{dt}} + \gamma\right)\right) - 2\omega \sin\left(2\omega \left(\frac{I_F}{\frac{dI_{D\,S}}{dt}} + \frac{V_{\mathrm{AKpk}} - V_d}{\frac{dV_{\mathrm{AK}}}{dt}} + \gamma\right)\right)}{((\alpha_I + \alpha_V)^2 + 4\omega^2)\, e^{(\alpha_I + \alpha_V)\left(\frac{IF}{\frac{dI_{\mathrm{DS}}}{dt}} + \frac{V_{\mathrm{AKpk}} - V_d}{\frac{dV_{\mathrm{AK}}}{dt}} + \gamma\right)}} \right. \right. \\ & \left. \left. - \frac{(\alpha_I + \alpha_V) \cos\left(2\omega \left(\frac{I_F}{\frac{dI_{\mathrm{DS}}}{dt}} + \frac{V_{\mathrm{AKpk}} - V_d}{\frac{dV_{\mathrm{AK}}}{dt}}\right) - 2\omega \sin\left(2\omega \left(\frac{I_F}{\frac{dI_{\mathrm{DS}}}{dt}} + \frac{V_{\mathrm{AKpk}} - V_d}{\frac{dV_{\mathrm{AK}}}{dt}}\right)\right)\right)}{\left((\alpha_I + \alpha_V)^2 + 4\omega^2\right) e^{(\alpha_I + \alpha_V)\left(\frac{I_F}{\frac{dI_{\mathrm{DS}}}{dt}} + \frac{V_{\mathrm{AKpk}} - V_d}{\frac{dV_{\mathrm{AK}}}{dt}}\right)}} \right) \right) \end{aligned} \tag{11}$$

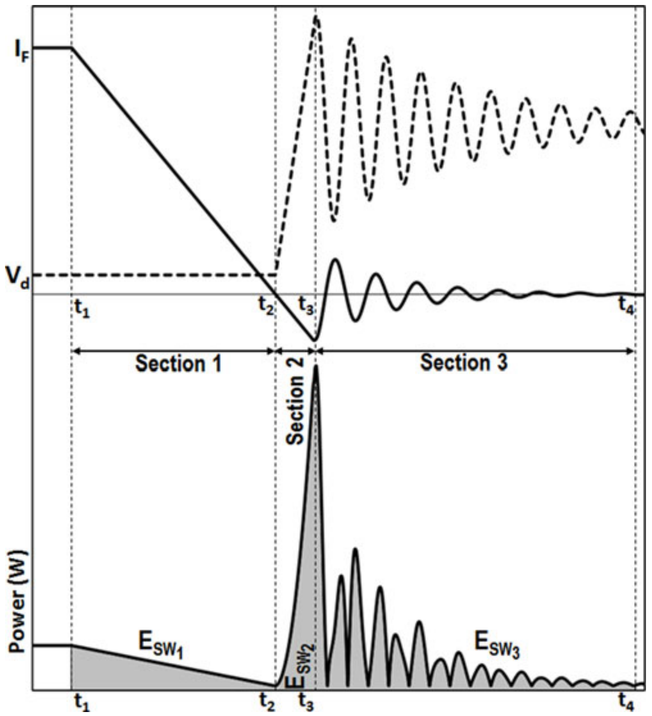

Fig. 10. Switching power in the model is divided into three distinct sections.

of the bottom-side MOSFET's dI_{DS}/dt is shown as (12), which is simply the derivative of (4) with respect to temperature

$$\frac{d^2 I_{\mathrm{DS}}}{dtdT} = \frac{V_{\mathrm{GG}}}{R_G C_{\mathrm{iss}}} \exp\left(-\frac{t}{R_G C_{\mathrm{iss}}}\right) \times \left((V_{\mathrm{GS}} - V_{\mathrm{TH}})\frac{\mathrm{dB}}{\mathrm{dT}} - B\frac{dV_{\mathrm{TH}}}{dT}\right). \quad (12)$$

The dependency of the MOSFETs gain factor (B) on temperature is due to the effective mobility's dependency on temperature. As the device temperature increases, phonon scattering reduces the effective mobility of the electrons in the MOSFET channel. This means that *dB/dT* is negative. The threshold voltage of a MOSFETis known to have a negative temperature coefficient due to the increase in the intrinsic carrier concentration as the temperature rises. The increase in the intrinsic carrier concentration, due to bandgap narrowing, means that the threshold voltage decreases as temperature increases since more carriers are available for subthreshold conduction. This means that dV_{TH}/dT is also negative. At lower temperatures, the temperature dependency of the threshold voltage dominates the temperature dependency of the effective mobility; hence, (12) can be rewritten as

$$\frac{\mathrm{d}^2 \mathrm{I}_{\mathrm{DS}}}{dtdT} = \frac{V_{\mathrm{GG}}}{R_G C_{\mathrm{iss}}} \exp\left(-\frac{t}{R_G C_{\mathrm{iss}}}\right)\left(B\left|\frac{\mathrm{dV}_{\mathrm{TH}}}{\mathrm{dT}}\right|\right). \quad (13)$$

Because the overall sign of (13) is positive, this means that the switching rate dI_{DS}/dt during MOSFET turn-ON increases with temperature as has already been demonstrated experimentally in Figs. 3 and 4.

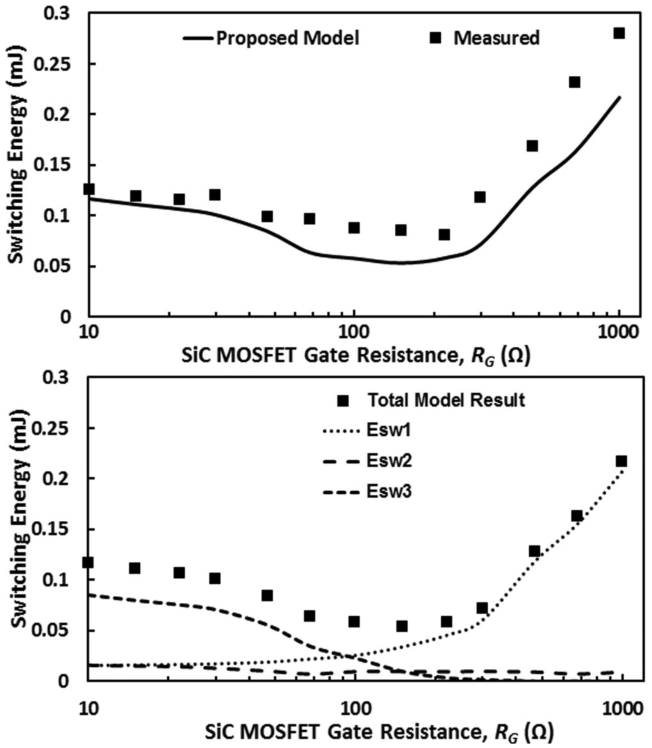

Fig. 11. Measured and the modeled switching energy as a function of the switching rate for each switching energy component ($E_{\mathrm{SW}1}$, $E_{\mathrm{SW}2}$, and $E_{\mathrm{SW}3}$) performed at room temperature.

Equation (14) describes the dependency of the switching rate on temperature

$$\frac{dI_{\mathrm{DS}}}{dt} = \frac{d^2 I_{\mathrm{DS}}}{dtdT}(T-25) + \left.\frac{dI_{\mathrm{DS}}}{dt}\right|_{T=25\,^\circ\mathrm{C}}. \quad (14)$$

The temperature dependency of the switching energy model is incorporated by substituting (14) as described below into the equation for E_{SWtotal}.

IV. Model Validation

The accuracy of the model is validated by comparing the predictions of the model with actual switching energy measurements. Fig. 11 shows the measured and calculated switching energy for the Schottky diode as a function of the switching rate (modulated by the gate resistances). It can be seen from Fig. 11(a) that the switching energy initially decreases as the switching rate is decreased. This is due to the fact diode ringing is better damped as the switching rate is reduced; hence, the additional power peaks arising from ringing are reduced. In this case, the switching energy of the voltage switching phase and the ringing phase ($E_{\mathrm{SW}2}$ and $E_{\mathrm{SW}3}$) in the developed model is the dominant factor in determining the total switching energy of the diode. As has been shown earlier, the switching energy of the ringing phase increases with dI_{DS}/dt. However, as the switching rate is further reduced, the switching energy starts to rise again. The oscillations are completely damped, so the total switching energy is now more dependent on the switching energy of the current switching phase $E_{\mathrm{SW}1}$, which increases

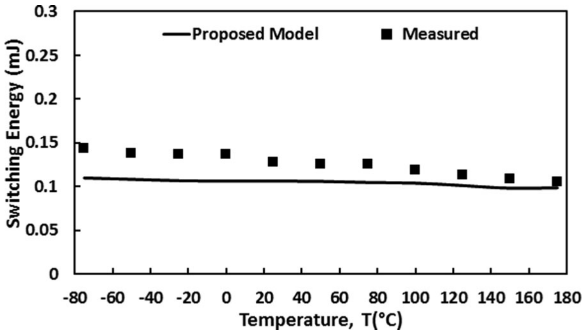

Fig. 12. Modeled and measured E_{SW} as a function of temperature ($R_{\mathrm{G}} = 15\ \Omega$).

as the switching rate is reduced. This is also predictable from the equations in the developed model for the switching energy. As seen, in (8), which describes the switching energy of the current switching phase, the dI_{DS}/dt is inversely proportional to the switching energy thereby causing the switching energy to decrease as the switching rate is increased (lower R_{G} is used). On the contrary, (9) is predicting that as dI_{DS}/dt and voltage overshoot V_{AKpk} is decreased, switching energy of voltage switching phase is also decreased. Measurements have shown that this is also correct since an increase in R_{G} results in a corresponding decrease in the dI_{DS}/dt and V_{AKpk}. Fig. 9 has also shown that the switching energy in ringing phase is reducing as the gate resistance increases due to damping of the oscillations. Fig. 11(b) shows total switching energy calculated broken down into the three components (E_{SW1}, E_{SW2}, and E_{SW3}). It can be seen from Fig. 11(b) that the E_{SW1} increases as the switching rate is reduced, while $\mathrm{E_{SW2}}$ and E_{SW3} decrease as the switching rate is decreased. The overall shape of the switching energy as a function of the switching rate is correctly predicted by the model. Fig. 12 shows the measured and calculated switching energy as a function of temperature. The switching energy is shown to be nearly temperature invariant, although there is a slight decrease with temperature observed and reasonably good agreement between the model and the measurements. This slight decrease is due to the fact that the oscillation is slightly damped at the diode output voltage as the temperature increases, which causes slight reduction in ringing losses. The model is correctly able to predict this because the temperature dependence of the switching rate has been incorporated into the diode switching energy model.

Fig. 13 shows the measured switching power transient at different temperatures for 10 Ω [in Fig. 13(a)], 47 Ω [in Fig. 13(b)], 100 Ω [in Fig. 13(c)], and 470 Ω [in Fig. 13(d)]. It can be seen from the measurements in Fig. 13 that the contribution of the switching energy of the current switching phase E_{SW1} increases with the gate resistance, whereas that of the voltage switching phase and the ringing phase (E_{SW2} and E_{SW3}) generally decreases as R_{G} is increased. The measurements show good agreement with the modeling. Fig. 14 shows the impact of switching rate and temperature on the switching energy of the SiC Schottky diode at (a) turn-ON (a) and (b) turn-OFF, where the U-shaped characteristics of Schottky diode in both cases can be seen. It can also be seen that the turn-ON switching energy is considerably smaller than the turn-OFF energy. Fig. 14 also shows that the dependency of the switching energy on temperature increases as the switching rate is reduced. At high switching rates, the switching energy is almost temperature invariant; however, as the switching rate is reduced,

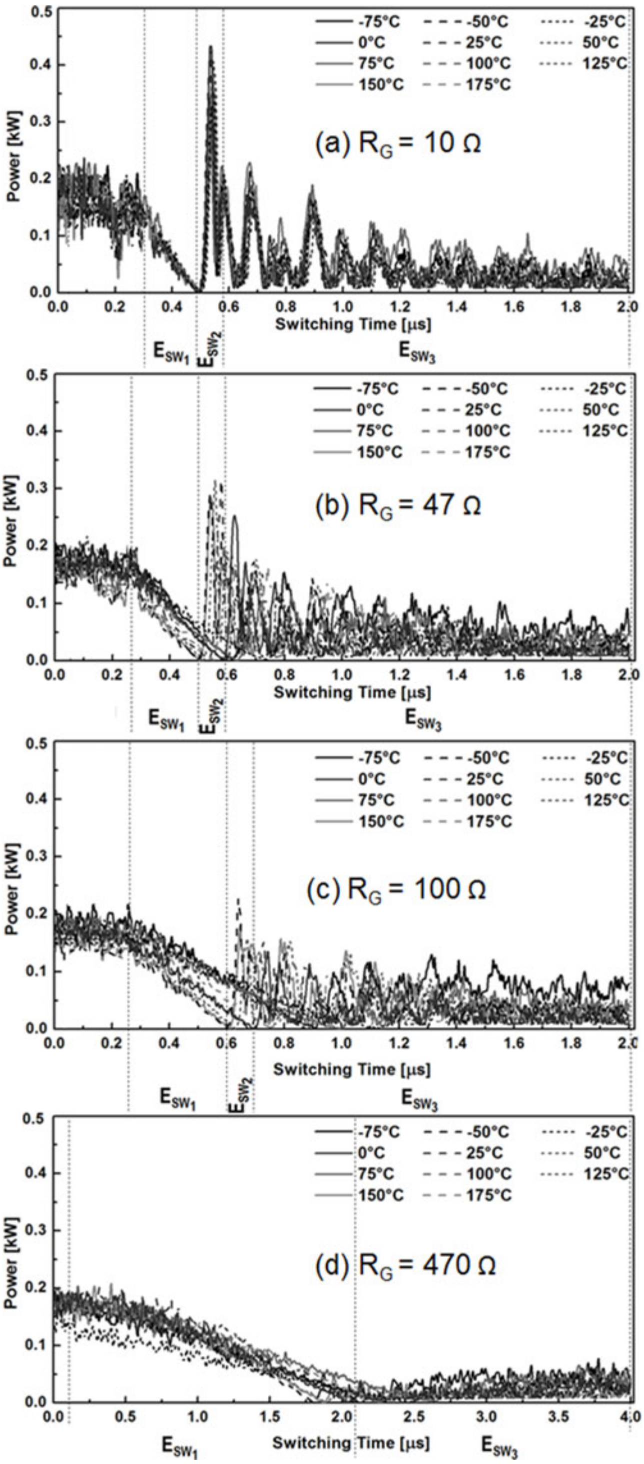

Fig. 13. Switching power transients for different temperatures and R_{G}.

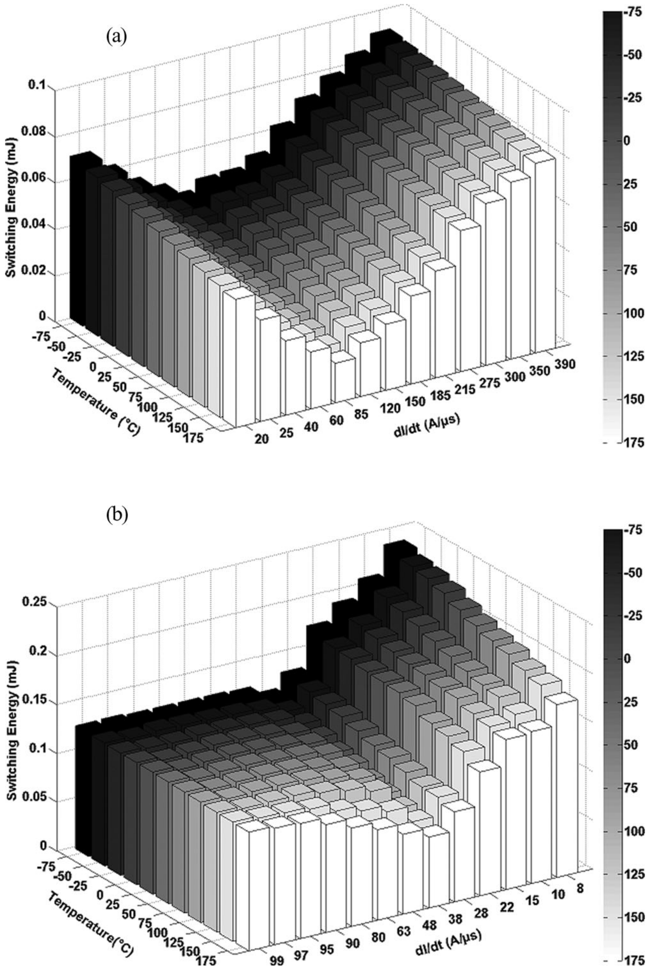

Fig. 14. (a) Turn-ON and (b) turn-OFF switching energy of the SiC Schottky diode as functions of the switching rate and temperature showing that the turn-OFF switching energy is much higher in magnitude. The measurements also show the U-shaped dependence of the switching energy on the switching rate.

the switching energy shows more of a temperature dependency. This was also correctly predicted in the model.

V. CONCLUSION

In this paper, a comprehensive model for the switching energy of the SiC Schottky diode is developed and validated through extensive measurements. The model for the diode switching energy is based on a thorough analysis of the diode ringing phenomenon and its temperature dependence. The results show convergence between the measurements and the model output with a considerably small margin of error. The switching energy of the diode is shown to be a combination of three switching phases namely the current switching phase, the voltage switching phase, and the ringing phase. While the switching energy of the current switching phase decreases with increasing switching rate, the switching energy of the voltage switching and the ringing phase increases with the switching rate (this is due to the fact that damping reduces as the switching rate increases; hence, the ringing losses dominate at high switching speeds). Hence, as the gate resistance that determines the switching speed of the low-side MOSFET is increased, the switching energy initially decreases as the ringing becomes better damped. However, beyond an optimum gate resistance, the switching energy starts increasing again because the switching energy of the current switching phase (which increases as the switching rate is reduced) starts to dominate the total switching energy. The developed models also predict the switching energy as a function of temperature. The temperature dependence of the switching energy increases as the switching rate is reduced.

REFERENCES

[1] M. Tarplee, V. Madangarli, Q. Zhang, and T. Sudarshan, "Design rules for field plate edge termination in sic schottky diodes," *IEEE Trans. Electron. Devices*, vol. 48, no. 12, pp. 2659–2664, Dec. 2001.

[2] D. Morisette, J. Cooper, J. A., M. Melloch, G. Dolny, P. Shenoy, M. Zafrani, and J. Gladish, "Static and dynamic characterization of large-area high-current-density sic schottky diodes," *IEEE Trans. Electron. Devices*, vol. 48, no. 2, pp. 349–352, Feb. 2001.

[3] K.-Y. Lee and Y.-H. Huang, "An investigation on barrier inhomogeneities of 4H-SiC Schottky barrier diodes induced by surface morphology and traps," *IEEE Trans. Electron. Devices*, vol. 59, no. 3, pp. 694–699, Mar. 2012.

[4] T. Funaki, J. Balda, J. Junghans, A. Kashyap, H. Mantooth, F. Barlow, T. Kimoto, and T. Hikihara, "Power conversion with sic devices at extremely high ambient temperatures," *IEEE Trans. Power Electron.*, vol. 22, no. 4, pp. 1321–1329, Jul. 2007.

[5] J. Nishio, C. Ota, T. Hatakeyama, T. Shinohe, K. Kojima, S.-I. Nishizawa, and H. Ohashi, "Ultralow-loss SiC floating junction schottky barrier diodes (super-SBDs)," *IEEE Trans. Electron. Devices*, vol. 55, no. 8, pp. 1954–1960, Aug. 2008.

[6] B. Ozpineci, M. Chinthavali, L. Tolbert, A. Kashyap, and H. Mantooth, "A 55-kw three-phase inverter with Si IGBTs and SiC Schottky diodes," *IEEE Trans. Ind. Appl.*, vol. 45, no. 1, pp. 278–285, Jan. 2009.

[7] C. Buttay, C. Raynaud, H. Morel, G. Civrac, M.-L. Locatelli, and F. Morel, "Thermal stability of silicon carbide power diodes," *IEEE Trans. Electron. Devices*, vol. 59, no. 3, pp. 761–769, Mar. 2012.

[8] J. Hefner, A. R., R. Singh, J.-S. Lai, D. Berning, S. Bouche, and C. Chapuy, "SiC power diodes provide breakthrough performance for a wide range of applications," *IEEE Trans. Power Electron.*, vol. 16, no. 2, pp. 273–280, Mar. 2001.

[9] G. Spiazzi, S. Buso, M. Citron, M. Corradin, and R. Pierobon, "Performance evaluation of a Schottky SiC power diode in a boost PFC application," *IEEE Trans. Power Electron.*, vol. 18, no. 6, pp. 1249–1253, Nov. 2003.

[10] Y. Du, J. Wang, G. Wang, and A. Huang, "Modeling of the high-frequency rectifier with 10-kV SiC JBS diodes in high-voltage series resonant type dc dc converters," *IEEE Trans. Power Electron.*, vol. 29, no. 8, pp. 4288–4300, Aug. 2014.

[11] J. Brown, "Modeling the switching performance of a MOSFET in the high side of a non-isolated buck converter," *IEEE Trans. Power Electron.*, vol. 21, no. 1, pp. 3–10, Jan. 2006.

[12] P. Godignon, X. Jorda, M. Vellvehi, X. Perpina, V. Banu, D. Lopez, J. Barbero, P. Brosselard, and S. Massetti, "SiC Schottky diodes for harsh environment space applications," *IEEE Trans. Ind. Electron.*, vol. 58, no. 7, pp. 2582–2590, Jul. 2011.

[13] Y. Liang, R. Oruganti, and T. Oh, "Design considerations of power MOSFET for high frequency synchronous rectification," *IEEE Trans. Power Electron.*, vol. 10, no. 3, pp. 388–395, May 1995.

[14] A. Vazquez, A. Rodriguez, M. Fernandez, M. Hernando, E. Maset, and J. Sebastian, "On the use of front-end cascode rectifiers based on normally on SiC JFET and Si MOSFET," *IEEE Trans. Power Electron.*, vol. 29, no. 5, pp. 2418–2427, May 2014.

[15] L. Lorenz, G. Deboy, and I. Zverev, "Matched pair of CoolMos transistor with SiC-Schottky diode—advantages in application," *IEEE Trans. Ind. Appl.*, vol. 40, no. 5, pp. 1265–1272, Sep. 2004.

[16] O. Guy, M. Lodzinski, A. Castaing, P. M. Igic, A. Perez-Tomas, M. Jennings, and P. Mawby, "Silicon carbide schottky diodes and mosfets: Solutions to performance problems," in *Proc. 13th Power Electron. Motion Control Conf.*, Sep. 2008, pp. 2464–2471.

[17] Z. Liang, P. Ning, and F. Wang, "Development of advanced all-sic power modules," *IEEE Trans. Power Electron.*, vol. 29, no. 5, pp. 2289–2295, May 2014.

[18] F. Xu, T. Han, D. Jiang, L. Tolbert, F. Wang, J. Nagashima, S. J. Kim, S. Kulkarni, and F. Barlow, "Development of a SiC JFET-based six-pack power module for a fully integrated inverter," *IEEE Trans. Power Electron.*, vol. 28, no. 3, pp. 1464–1478, Mar. 2013.

[19] R. Singh, J. Cooper, J. A., M. Melloch, T. Chow, and J. Palmour, "SiC power Schottky and pin diodes," *IEEE Trans. Electron. Devices*, vol. 49, no. 4, pp. 665–672, Apr. 2002.

[20] B. Ozpineci and L. Tolbert, "Characterization of SiC Schottky diodes at different temperatures," *IEEE Power Electron Lett.*, vol. 1, no. 2, pp. 54–57, Jun. 2003.

[21] A. Bryant, L. Lu, E. Santi, P. Palmer, and J. Hudgins, "Physical modeling of fast p-i-n diodes with carrier lifetime zoning, part i: Device model," *IEEE Trans. Power Electron.*, vol. 23, no. 1, pp. 189–197, Jan. 2008.

[22] L. Lu, A. Bryant, E. Santi, P. Palmer, and J. Hudgins, "Physical modeling of fast p-i-n diodes with carrier lifetime zoning, part ii: Parameter extraction," *IEEE Trans. Power Electron.*, vol. 23, no. 1, pp. 198–205, Jan. 2008.

[23] H. Wang, E. Napoli, and F. Udrea, "Breakdown voltage for superjunction power devices with charge imbalance: An analytical model valid for both punch through and non punch through devices," *IEEE Trans. Electron. Devices*, vol. 56, no. 12, pp. 3175–3183, Dec. 2009.

[24] S. Bellone, F. Della Corte, L. Albanese, and F. Pezzimenti, "An analytical model of the forward i v characteristics of 4h-sic p-i-n diodes valid for a wide range of temperature and current," *IEEE Trans. Power Electron.*, vol. 26, no. 10, pp. 2835–2843, Oct. 2011.

[25] S. Bellone, F. Della Corte, L. Di Benedetto, and G. Licciardo, "An analytical model of the switching behavior of 4h-sic p+nn+ diodes from arbitrary injection conditions," *IEEE Trans. Power Electron.*, vol. 27, no. 3, pp. 1641–1652, Mar. 2012.

[26] T. McNutt, J. Hefner, A.R., H. Mantooth, J. Duliere, D. Berning, and R. Singh, "Silicon carbide pin and merged pin schottky power diode models implemented in the saber circuit simulator," *IEEE Trans. Power Electron.*, vol. 19, no. 3, pp. 573–581, May 2004.

[27] G. Buiatti, F. Cappelluti, and G. Ghione, "Physics-based pin diode spice model for power-circuit simulation," *IEEE Trans. Ind. Appl.*, vol. 43, no. 4, pp. 911–919, Jul. 2007.

[28] D. Morisette and J. Cooper, J. A.,"Theoretical comparison of sic pin and schottky diodes based on power dissipation considerations," *IEEE Trans. Electron. Devices*, vol. 49, no. 9, pp. 1657–1664, Sep. 2002.

[29] G. Brezeanu, M. Badila, B. Tudor, J. Millan, P. Godignon, F. Udrea, G. Amaratunga, and A. Mihaila, "Accurate modeling and parameter extraction for 6H-SiC Schottky barrier diodes (SBDs) with nearly ideal breakdown voltage," *IEEE Trans. Electron. Devices*, vol. 48, no. 9, pp. 2148–2153, Sep. 2001.

[30] O. Alatise, N.-A. Parker-Allotey, D. Hamilton, and P. Mawby, "The impact of parasitic inductance on the performance of siliconcarbide schottky barrier diodes," *IEEE Trans. Power Electron.*, vol. 27, no. 8, pp. 3826–3833, Aug. 2012.

[31] S. Jahdi, O. Alatise, P. Alexakis, L. Ran, and P. Mawby, "The impact of temperature and switching rate on the dynamic characteristics of silicon carbide Schottky barrier diodes and MOSFETS," *IEEE Trans. Ind. Electron.*, vol. PP, no. 99, pp. 1–1, 2014.

[32] S. Jahdi, O. Alatise, C. Fisher, L. Ran, and P. Mawby, "An evaluation of silicon carbide unipolar technologies for electric vehicle drive-trains," *IEEE J. Emerg. Sel. Topics iPower Electron.*, vol. 2, no. 3, pp. 1–12, Jun. 2014.

Saeed Jahdi (S'10) received the B.Sc. degree in electrical power engineering from the University of Science and Technology, Tehran, Iran, in 2005, and the M.Sc. degree with distinction in power systems and energy management from City University London, London, U.K., in 2012.

Since then, he has been working toward the Ph.D. degree in electrical engineering at Power Electronics Laboratory, School of Engineering, University of Warwick, Coventry, U.K., while he has been awarded an energy theme scholarship for the duration of his research. His current research interests include wide band-gap semiconductor devices in high-voltage power converters, circuits, and applications.

Mr. Jahdi is a Member of the IEEE Power Electronics and Industrial Electronics Societies.

Olayiwola Alatise (M'05) received the B.Eng. degree (with first-class Hons.) in electrical and electronic engineering and the Ph.D. degree in microelectronics and semiconductors from Newcastle University, Newcastle upon Tyne, U.K., in 2008.

His research focused on mixed-signal performance enhancements in strained Si/SiGe metaloxidesemiconductor field-effect transistors (MOSFETs). In 2004 and 2005, he briefly joined Atmel North Tyneside, where he worked on the process integration of the 130-nm CMOS technology node. In June 2008, he joined the Innovation R&D Department, NXP Semiconductors, as a Development Engineer, where he designed, processed, and qualified discrete power trench MOSFETs for automotive applications and switched-mode power supplies. In November 2010, he became a Science City Research Fellow with the University of Warwick and since August 2012, he has been serving as an Assistant Professor of electrical engineering at the University of Warwick, Coventry, U.K. His research interest include investigating advanced power semiconductor materials and devices for improved energy conversion efficiency.

Li Ran (M'98–SM'07) received the Ph.D. degree in power systems engineering from Chongqing University, Chongqing, China, in 1989.

He was a Research Associate with the Universities of Aberdeen, Nottingham and Heriot-Watt, at Aberdeen, Nottingham, and Edinburgh, U.K., respectively. He became a Lecturer in Power Electronics with Northumbria University, Newcastle upon Tyne, U.K., in 1999 and was seconded to Alstom Power Conversion, Kidsgrove, U.K., in 2001. Between 2003 and 2012, he was with Durham University, Durham, U.K. He joined the University of Warwick, Coventry, U.K., as a Professor in power electronics - systems in 2012. His research interests include the application of power electronics for electric power generation, delivery, and utilization.

Philip Mawby (S'85–M'86–SM'01) received the B.Sc. and Ph.D. degrees in electronic and electrical engineering from the University of Leeds, Leeds, U.K., in 1983 and 1987, respectively. His Ph.D. dissertation was focused on GaAs/AlGaAs heterojunction bipolar transistors for high-power radio frequency applications at the GEC Hirst Research Centre, Wembley, U.K.

In 2005, he joined the University of Warwick, Coventry, U.K., as the Chair of power electronics. He was also with the University of Wales, Swansea, U.K., for 19 years and held the Royal Academy of Engineering Chair for power electronics, where he established the Power Electronics Design Center, which has been involved in a whole range of areas relating to power electronics and interaction with small and medium enterprises in Wales as well as larger international companies. He has been internationally recognized in the areas of power electronics and power device research. He was also involved in the development of device simulation algorithms, as well as optoelectronic and quantum-based device structures. He has authored or coauthored more than 70 journal papers and 100 conference papers. His current research interests include materials for new power devices, modeling of power devices and circuits, and power-integrated circuits.

Dr. Mawby has been involved in many international conference committees, including the International Symposium on Power Semiconductor Devices, the European Power Electronics, the Bipolar/BiCMOS Circuits and Technology Meeting, and the European Solid-State Device Research Conference. He is a Chartered Engineer, a Fellow of the Institution of Engineering and Technology, and a Fellow of the Institute Physics. He is a Distinguished Lecturer for the IEEE Electron Devices Society.